Cement & Concrete Composites 34 (2012) 936–945

Contents lists available at SciVerse ScienceDirect

Cement & Concrete Composites

journal homepage: www.elsevier.com/locate/cemconcomp

The role of hydrotalcite in chloride binding and corrosion protection in concretes with ground granulated blast furnace slag

Obada Kayali [a,*], M.S.H. Khan [a], M. Sharfuddin Ahmed [b]

[a] School of Engineering and Information Technology, University of New South Wales at The Australian Defence Force Academy, Canberra, Australia
[b] Roads ACT, Territory and Municipal Directorate, Canberra, Australia

ARTICLE INFO

Article history:
Received 24 January 2012
Received in revised form 20 April 2012
Accepted 24 April 2012
Available online 3 May 2012

Keywords:
Chloride
Corrosion
Slag
Hydrotalcite
Friedel's salt
Silica fume

ABSTRACT

This paper presents an investigation into the extent and reasons of the observed improvement in performance that ground granulated blast furnace slag (GGBFS) contributes against chloride initiated corrosion. Tests conducted on concretes with blended cement included Rapid Chloride Permeability Test (RCPT), long term ponding, corrosion current monitoring, pore size distribution and X-ray diffraction analyses. Values of the RCPT and corrosion current were significantly reduced as the proportion of GGBFS increased. The results showed only small refinements in pore size distribution, as well as indications of the formation of Friedel's salt. The tests however, revealed the formation of hydrotalcite as a significant hydration product in GGBFS blends. The results further demonstrated the efficiency of hydrotalcite in binding chloride ions. The authors attribute the reduction in corrosion current to the efficient binding of chloride ions by the hydrotalcite that forms in GGBFS hydration products.

1. Introduction

The recent thrust for creating sustainable concrete structures has brought particular attention to the many advantages that the concrete industry can gain from including industrial by-products that possess pozzolanic properties in their mixtures [1]. High strength-high performance concrete has become somewhat synonymous with the inclusion of silica fume at a proportion that has been optimised at around slightly less than 10% of the total binder content on a mass basis [2–4]. Quite recently, ternary blends containing combinations of OPC, silica fume, fly ash and GGBFS have started to become more thoroughly investigated [5,6]. Clearly, the purpose of such binary or ternary mixture is to harness the most desirable properties suitable for the intended construction. Evidence of better corrosion performance of concretes with binary and ternary blends has recently been supported by various investigators [6,7]. Naturally, attention has been directed towards the performance of the pozzolanic industrial by-product materials in environments conducive to the corrosion of embedded steel. Hence the effects of such materials on the microstructural, chemical and physical properties are of paramount importance. The use of materials such as fly ash, silica fume or GGBFS, has been shown to significantly affect the pore solution chemistry and consequently, the electrical conductivity [8–10]. The beneficial effects of GGBFS, especially in aggressive chloride and/or sulphate rich environments, have been well documented and GGBFS is therefore, regarded as an effective means in producing high performance concrete [1,11,12]. Dhir et al. [13] investigated the chloride binding capacity of paste containing GGBFS at different replacement levels and concluded that it increased with the increase of GGBFS content. They also found that the binding capacity of the paste at 66.7% GGBFS content was about five times that of plain Portland cement paste. Dhir et al. as well as Luo et al. attributed this capability to increased formation of Friedel's salt [13,14].

However, the chemical constituents of GGBFS differ considerably from that of Portland cement, fly ash and silica fume, and notably in the amount of magnesia [15]. Subsequently, magnesia contributes to form hydrotalcite in significant amounts during hydration [16,17]. Hydrotalcite is one of the most representative minerals of the Layered Double Hydroxides (LDHs) group. It occurs both naturally and synthetically and has the chemical formula of $Mg_6Al_2(OH)_{16}CO_3{\cdot}4H_2O$. However, the chemical formula of hydrotalcite may change depending on the molar ratio $Al^{3+}/(Mg^{2+} + Al^{3+})$ which varies from 0.2 to 0.33 [18]. Hydrotalcite consists of divalent and trivalent cations dispersed amongst the octahedral layers to form positively charged layers. The negatively charged anions are housed in the interlayer between the positively charged layers [19]. A distinctive and valuable characteristic of hydrotalcite lies in its anion exchange property by which the interlayer anions can be replaced with a wide range of inorganic and organic anions [20]. Hydrotalcite's anion exchange property has been effectively used to neutralise acids in the stomach [21] or to resist corrosion

* Corresponding author. Tel.: +61 2 62688329; fax: +61 2 62688337.
E-mail address: o.kayali@adfa.edu.au (O. Kayali).

0958-9465/$ - see front matter © 2012 Elsevier Ltd. All rights reserved.
http://dx.doi.org/10.1016/j.cemconcomp.2012.04.009

on metal surfaces [22,23]. Hybrid sol-gel coatings with hydrotalcite are effective in improving mechanical and physical properties of metal surfaces, including resistance against corrosion. When the coated surface is exposed to salt attack, the attacking chloride ion is adsorbed by hydrotalcite and thus the surface gets protection against corrosion [24,25]. Based on the reported evidence on the properties of hydrotalcite and in particular, its ion exchange capability, the authors decided to examine this capability in GGBFS concrete. In particular, the authors aimed to examine the apparent capability of GGBFS to bind chloride ions, and investigate whether formation of hydrotalcite is involved in making a significant drop in the free chloride ion content in concrete. First, the paper presents the effects of binary and ternary blends of Portland cement, silica fume and GGBFS on the chloride penetration and the chloride initiated corrosion. The study employed the RCPT, the salt solution long-term ponding test, corrosion current measurement and pore size distribution analysis in order to determine whether there is a correlation between results of these indicators. The authors subsequently discuss the possible reasons causing the enhanced binding of chloride ions in such concretes and resulting in lower corrosion currents. X-ray diffraction (XRD) was employed to analyse qualitatively and quantitatively the extent of hydrotalcite formation in GGBFS hydration products. Furthermore, pure hydrotalcite was exposed to chloride solutions and its capability to bind chloride ions was investigated using chemical and XRD analyses. These methods helped to shed light on an important role that hydrotalcite may play in protection against corrosion in reinforced concrete.

2. Materials and testing

2.1. Materials

Crushed dacite coarse aggregates of 9.5 mm maximum size, complying with ASTM C 33, were used. The aggregates were washed and dried before casting. Washed river bed sand was used as fine aggregates. Concrete mixtures were cast with a total cementitious materials content of 450 kg/m^3. The OPC was replaced with low, medium, and high percentages of GGBFS at the replacement levels of 25%, 50%, and 70% by mass. Silica fume was used at 10% replacement of the total cementitious materials content in all the ternary mixes. Pure hydrotalcite was obtained from Sigma–Aldrich chemical company. Its chemical analysis, as well as the chemical analyses of OPC, silica fume, and GGBFS used in this series, is shown in Table 1. The hydrotalcite needed for making the mixes used for measuring chloride adsorbing capacity as well as XRD testing, was calcined according to the method of Lv et al. [26], by which the hydrotalcite was placed in a furnace for 3 h at 500 °C before cooling down to room temperature. It was then kept in a sealed container until testing, to prevent any contamination.

Table 1
Chemical and physical properties of OPC, SF, GGBFS and hydrotalcite.

Chemical and physical properties	Cement (%)	SF (%)	GGBFS (%)	Hydrotalcite (%)
SiO_2	21.1	>90	34.1	0.15
Al_2O_3	5.2	<0.9	13.2	19.19
Fe_2O_3	4.3	<1.5	0.7	–
CaO	64.2	<0.4	41.8	0.09
MgO	1.2	<0.1	6.3	34.32
Na_2O, K_2O	0.05, 0.47	<0.4, <0.9	0.27, 0.34	–
SO_3	2.6	<0.03	2.4	–
Loss of ignition	0.8	–	0.5	46.05
Specific gravity	3.13	2.24	2.86	2
Fineness index (m^2/kg)	350	23,500	425	–

2.2. Concrete mixes

A total of 8 types of mixes were cast using constant water to binder (w/b) mass ratio of 0.38 and varying the dosage of superplasticizer to obtain similar workability characteristics reflected in slump values in the range of 80–120 mm. A polycarboxylic ether superplasticizer usually used in producing high performance concrete was used in this series. The mixes were designated as follows: The letters C, S, and B stand for OPC, silica fume, and GGBFS, respectively. For example, in the mix CB7S, C represents ordinary Portland cement, B7 represents 70% replacement of the total binder by GGBFS, and S represents 10% replacement of the total binder by silica fume. Likewise, in CB2S, B2 represents 25% replacement of the binder by GGBFS. The fresh and hardened concrete properties of all mixes are reported in Table 2.

2.3. Slab specimens

A reinforced concrete slab panel of size 500 × 500 × 60 mm was cast for each mix. The concrete cover at the top and bottom were 30 and 15 mm, respectively. The slabs were air dried in the laboratory for a period of 28 days after one week of fog curing. On the 29th day, the slabs were ponded with 3% sodium chloride solution (chloride ion concentration of 18,198 ppm) placed on the top of the slab with an average depth of 10 mm. The slabs were placed in a room where the ambient temperature and RH were 23 °C and 40%, respectively. Marine grade aluminium was used to enclose the sodium chloride solution on top of the slabs. The sodium chloride solution was completely removed on a weekly basis and was replenished with freshly prepared solution. The solution was continually stirred to avoid stratification. The ponding period lasted for 710 days, after which concrete powder specimens were extracted from the range of 25–45 mm depth, which represents the reinforcement vicinity.

Table 2
Mix quantities* and fresh and mature properties of mixes; w/b: 0.38.

Materials and properties	OPC	CS	CB2	CB2S	CB5	CB5S	CB7	CB7S
Cement (kg/m^3)	450	405	337.5	292.5	225	180	135	90
Silica fume (kg/m^3)	–	45	–	45	–	45	–	45
Blast furnace slag (kg/m^3)	–	–	112.5	112.5	225	225	315	315
Total cementitious content (kg/m^3)	450	450	450	450	450	450	450	450
Coarse aggregate (kg/m^3) – (oven dried)	1110	1101	1105	1096	1100	1091	1111	1102
Fine aggregate (kg/m^3) – (oven dried)	680	675	677	672	674	669	681	675
Superplasticizer L/100 kg binder	1.14	1.3	1.3	1.31	1.2	1.3	0.94	1.3
Water-effective (kg) – (free)	171	171	171	171	171	171	171	171
Slump (mm)	65	85	200	90	35	130	155	110
Air content (%)	1.65	0.9	0.35	1.4	0.7	1.15	0.75	1.15
Hardened concrete density (kg/m^3) – 365 days	2360	2344	2357	2330	2341	2318	2361	2324
Compressive strength (MPa) 365 days	76.8	73.4	68.5	64.3	55.6	53.2	58.6	56.9

* Aggregates quantities are in the oven dry condition, while the shown water quantity is the free water after absorption has occurred.

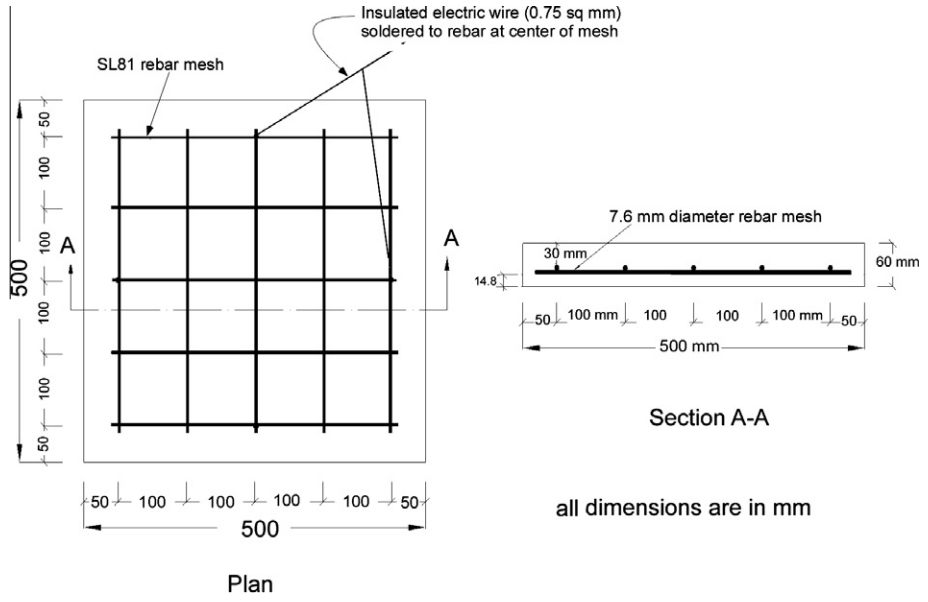

Fig. 1. Details of the reinforced concrete slab.

The samples were analysed for acid soluble chlorides following the AASHTO-T260 method [27]. Details of slab and reinforcement are shown in Fig. 1.

2.4. RCPT specimens

The Rapid Chloride Permeability Test (RCPT) has been used as a standard test to evaluate the susceptibility of certain concretes to chloride initiated reinforcement corrosion [28,29]. It was however, argued that the RCPT is more a measure of resistivity to electric current rather than a chloride ion permeability test [30,31]. Researchers have advocated the use where appropriate, of the long term ponding test [32] as a better representation of chloride penetration [33]. Indeed, the latter test presents a reliable method for quantifying total chloride ingress, as well as being suitable for measuring corrosion current in ponded reinforced slabs [34]. For each mix, 8 disc specimens (with the exception of the control mix which had seven specimens) of 100 mm diameter and 50 mm thickness were cast. The specimens were demoulded 24 h after casting and were fog cured for a period of 7 days. They were then exposed in an environmental room maintained at 23 °C and 50% RH. The test was performed after 350 days, following the procedures outlined in AASHTO-T277.

2.5. Pore size distribution analysis

Pore size distribution analysis was performed on samples collected from the central core of compressive strength cylinders crushed after one year of casting. The specimens were kept in vacuum desiccators over silica gel. Pore size distribution determination was performed using the nitrogen adsorption porosimetry method.

2.6. Measurement of hydrotalcite's chloride adsorbing capacity

For this purpose, a procedure proposed by Wajima et al. was adopted [35]. Accordingly, calcined hydrotalcite was added to 80 mL NaCl solution containing 3% NaCl by mass (representing average content in sea water). The mixture was stirred for several hours to allow for the reaction between chlorides and hydrotalcite. The mixture was then filtered and the concentration of chloride in the filtrate solution was determined using a chloride ion selective electrode. The reduction in the concentration of the original solution is due to hydrotalcite adsorption of chloride ions. The adsorption capacity was determined in two steps. The first step is done in order to determine the optimum length of time needed for the reaction. For this purpose, 8 g of calcined hydrotalcite were added to 80 mL NaCl solution and the reaction time was varied from 1 h to 24 h. In the second step, the dose of calcined hydrotalcite was varied while keeping a constant reaction time as obtained in the first step.

2.7. Investigation using X-ray diffraction

X-ray diffraction (XRD) investigation was carried out to:

(1) Identify hydrotalcite formation during hydration of plain GGBFS. For this purpose, plain GGBFS was activated with 4 M NaOH to accelerate hydration reactions. This mixture is referred to here as 4M_GGBFS.
(2) Investigate whether Friedel's salt is also formed as a result of activating plain GGBFS and subsequent contact with chlorides. For this purpose, NaCl constituting 2.47% by dry mass of GGBFS (to make 1.5% of Cl^- ion by GGBFS mass) was dissolved into the quantity of 4 M NaOH solution required for making the GGBFS paste.
(3) Identify whether there is hydrotalcite formation in hardened binary blend paste of ordinary Portland cement and GGBFS. For this purpose, a paste consisting of 50% GGBFS by mass of cementitious material was cast. This mixture is referred to here as 4M_GGBFS50. The mixture was also activated with 4M NaOH.

All types of GGBFS pastes in 1, 2 and 3 above were cast in plastic vials with sealing caps and using a liquid to binder (w/b) ratio of 0.35. The samples were demoulded after 24 h and subsequently placed in a controlled environment room at 50% relative humidity and 23 °C until testing.

(4) Investigate whether other identifiable crystalline compounds form as a result of interaction between the hydrotalcite and NaCl. For this purpose, NaCl was added to plain calcined

hydrotalcite. The method applied by Wajima et al. [35] to measure the chloride binding ability of hydrotalcite, as outlined in Section 2.6, was also adopted here. In this procedure, 16 g of calcined hydrotalcite were added to 80 mL of NaCl solution containing 3% NaCl by mass. The mix was stirred for 24 h then filtered. The residual solids were dried in an oven at 105 °C for 24 h. The dried solids were then ground to a powder and kept in sealed condition until XRD testing.

(5) Quantify the relative proportion of the hydrotalcite phase. This was done using the computer program Rietica [36] that is based on the Rietveld method [37]. This method has been successfully used in the quantification of cement clinker [38] minerals as well as cement hydration products [39]. The software's algorithm performs the analysis and calculations of the proportions of the minerals that are present in crystalline form.

At the time of analysis, the samples were crushed to fine powder. The diffraction conditions were: 40 kV, 25 mA, Cu Kα radiation with wavelength 0.15418 nm, scan range 5°–65°, 0.1° 2θ step size with speed of 1°/min.

2.8. Corrosion measurement

The corrosion evaluation was performed using a "GECOR6" corrosion rate metre developed by GEOCISA in collaboration with two leading Spanish research centres. The apparatus works on the principle of linear polarization [40]. The corrosion rate is measured in terms of the corrosion current density, I_{corr} and is expressed in microamperes per square centimetre (μA/cm^2). Values between (0.1 and 1 μA/cm^2) are the most frequently observed. A corrosion current density less than 0.1 μA/cm^2 is associated with passivity or negligible corrosion activity [41]. The corrosion rate for all slab reinforcement was monitored for the total exposure period of 710 days. The results presented here are those recorded at the conclusion of the testing period. Each result represents the average of 12 measured values.

3. Results and discussion

3.1. Effect on induced electrical charge

The results plotted in Fig. 2 shows that replacing cement with increasing proportions of GGBFS up to 50% of the binding material has decreased the electric charge passed in RCPT evaluations. However, when the proportion of GGBFS was 70% there appears to be a reversal of the trend. This is not surprising because it is expected that such a high replacement level may produce less overall reaction, resulting in a less dense internal structure and more interconnected pores that would facilitate ion mobility. Thus, the ability of GGBFS concrete to resist passing of electric charge may start to become increasingly counterbalanced by any increase in the interconnected porosity. Nevertheless, even at the 70% replacement level, the GGBFS concrete was more resistant to the passing of current than plain OPC concrete. In the binary blends of OPC and GGBFS, a maximum reduction of 36% in electric charge was obtained (compared to the OPC control) when the GGBFS constituted 50% of the total binder. The 10% replacement of Portland cement by silica fume has also decreased the charge. It is observed that replacing 10% of cement by silica fume has resulted in a 50% reduction in charge compared to plain OPC concrete. In ternary blends with both GGBFS and silica fume, it is observed that silica fume could further decrease the charge passed even below the level obtained with binary blends with GGBFS. Ternary blends where GGBFS proportion was 25%, have also showed lower charge than

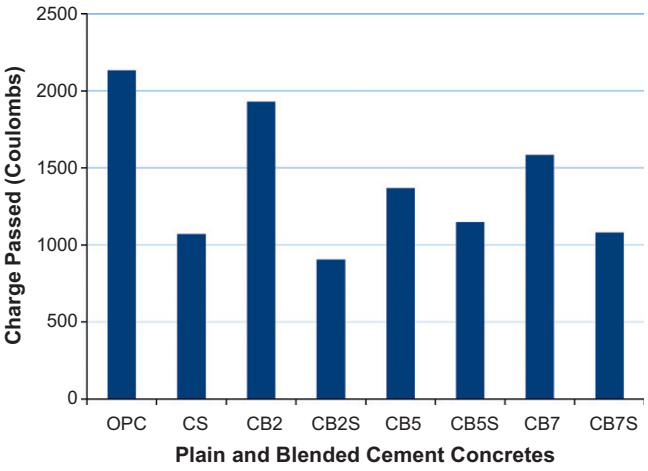

Fig. 2. Charge passed in the RCPT after 350 days of controlled environment exposure.

in binary blends of OPC and silica fume. A maximum reduction of 58% has occurred in the ternary blend where the GGBFS and silica fume constituted 25% and 10% of the binder, respectively. The above discussed results and observations clearly indicate that the charge passed in the RCPT may be strongly affected by changes that would occur in the pore solution's chemical composition as a result of the inclusion of pozzolanic materials. The availability of mobile ions in the pore solution that is present in interconnected pores is expected to facilitate the passing of electrical current. It is therefore reasonable to expect that the less the quantity of mobile Cl^- ions is, the lower would the conductivity be. Indeed, if the pozzolanic materials could bind, and thus immobilise such ions, a less quantity of free Cl^- ions would be present in the pore solution, thus resulting in lower conductivity. In the sections to follow, this hypothesis is examined through investigating the ability of GGBFS to bind chloride as a consequence of hydrotalcite formation being one of its main hydration products.

It is interesting, that such an indication of high performance is not accompanied by an increase in strength. On the contrary, it can be seen (Table 2) that the strength of the OPC control has been the highest and has progressively decreased as the pozzolanic material replacement increased. Yet, the compressive strength of the binary blend with only 30% OPC was around 59 MPa compared to around 77 MPa for the 100% OPC. Although this is not exactly the subject of this paper, the authors see it appropriate to draw attention to the benefits of being able to so significantly reduce the amount of Portland cement and at the same time improve the quality of concrete through better durability performance, while still keeping an acceptable high strength level. Nevertheless, it is important to note that at the level of silica fume replacement being 10% of the total cementitious materials' content, there has been an observed consistent decrease in strength in all the tested combinations (Table 2). This has been the case despite an equally consistent reduction in the passed electrical charge, evidently resulting from micro-silica presence as can be seen in Fig. 2.

3.2. Effect on total Cl^- content near the reinforcement

Results of total chloride content analysis are shown in Fig. 3. The results for the slabs within the depth of 25–45 mm, ponded under chloride solution showed that the total chloride content in all the concretes ranged between 0.21% and 0.28% of the binder mass. Fig. 3 shows a trend of slightly decreasing chloride content as the GGBFS replacement proportion increases. It should be noted that this measured chloride is the total chloride that managed to

permeate to this particular depth. This includes both the free and the bound chlorides. It may therefore be concluded that it is the total chloride content that reflects the chloride permeability of the concrete and is mainly affected by its porosity characteristics. Nevertheless, the pore size distribution shown in Fig. 4 does not indicate a consistent or conclusive trend although the curves of all the mixtures seem to be in close proximity. Moreover, it must be noted that keeping a constant w/b mass ratio while also keeping a constant total binder mass, results in alteration to the initial water filled porosity of the different mixtures. This is mainly due to the lower density values of the pozzolanic materials which in turn results in these materials occupying a slightly larger solid volume than in the case of plain Portland cement. This may well affect the pores distribution characteristics. The authors therefore, attribute the slightly decreasing trend in the total chloride content in the pozzolanic blends, as illustrated in Fig. 3, to a reduction in general permeability owing to a reduction in the volume of available pores.

It is also worth noting that previous studies of the pore solution chemistry of silica fume as well as GGBFS cement blends showed that the free chloride concentration increases significantly as a result of silica fume addition [42] and decreases steeply as a result of GGBFS blending [43]. On the other hand, the free chloride concentration reflects the capability of the pozzolanic material to bind chloride ions, in the case of GGBFS, or its capability to dissociate the already bound chloride as seems to be the case with silica fume blends. Indeed, there has been plenty of evidence that the addition of silica fume results in the decomposition of Friedel's salt [10,42].

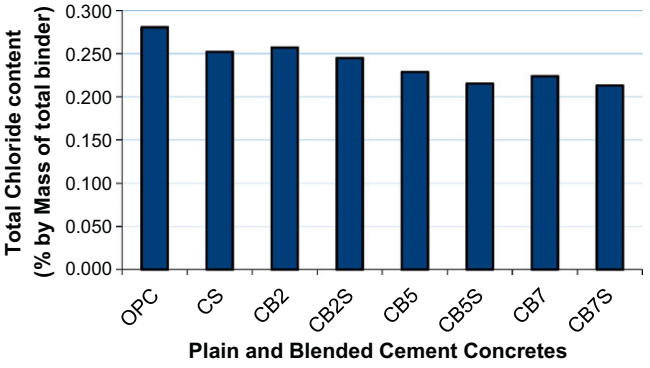

Fig. 3. Total chloride content at 25–45 mm depth after 2 year ponding.

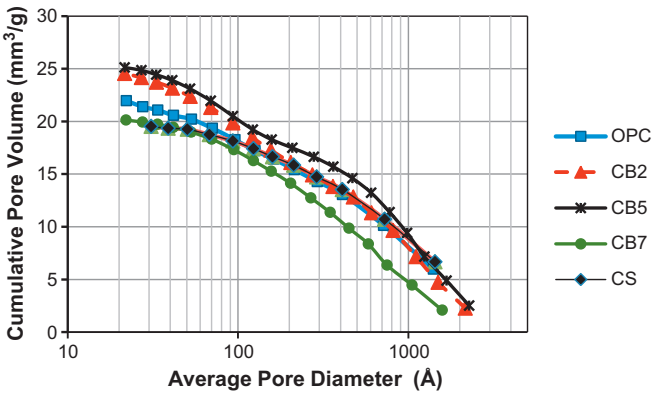

Fig. 4. Pore size distribution of OPC and binary blend concretes after 350 days of controlled environment exposure. (1 Å = 0.1 nm).

3.3. Effect on the OH^- concentration

There is overwhelming evidence that the OH^- concentration substantially decreases in the pore solution of concretes with GGBFS, fly ash or microsilica [10,43–48]. Vedalakshmi et al. [43] have found that OH^- ion concentration in GGBFS concrete decreases to about half its value in plain OPC concrete. Rasheeduzzafar and Ehtesham Hussain concluded that GGBFS acts as an alkali diluent and that 60% slag cement is equivalent in its alkali removal to 10% microsilica cement [49]. Rasheeduzzafar et al. [42] have also shown that 10% substitution of cement by microsilica resulted in doubling the free chloride ion concentration in the pore solution. The increase in Cl^- concentration was accompanied by a large decrease in the concentration of OH^-. Subsequently a very high value of Cl^-/OH^- ratio resulted. It has been known that Cl^- ions get bound in cement paste as a result of the C_3A and C_4AF presence. C_3A and C_4AF hydrates bind chloride ions in Friedel's salt ($3CaO{\cdot}Al_2O_3{\cdot}CaCl_2{\cdot}10H_2O$) [42,50–52] and its ferrite phase form ($3CaO{\cdot}Fe_2O_3{\cdot}CaCl_2{\cdot}10H_2O$) [42,51]. Such binding is thought to be dissociated as a consequence of silica fume addition and hence resulting in the increase of free Cl^- concentration [10,42]. The increase in free Cl^- concentration in microsilica cement has been attributed to the lower alkalinity in microsilica cement blends [10], although this issue is still quite controversial [42,53]. The expectation was that such an environment would result in high activity of chloride initiated corrosion. Nevertheless, results of those researchers, as well as the present authors, have shown that in the cases of binary and ternary blends involving silica fume and GGBFS, corrosion current was far less in the blended cement concretes than it was in the plain concrete.

Vedalakshmi et al. [43] have found that concrete with GGBFS blended cement exhibited a large reduction in the free chloride content. The reduction exceeded 50% compared to plain OPC concrete. Vedalakshmi et al. [43] have also found a substantial reduction in the OH^- ion concentration. However they reported that such a reduction in the OH^- ion concentration did not adversely affect corrosion of reinforcing steel. Several researchers have also demonstrated that the inclusion of GGBFS results in reduced chloride ion concentrations [13,14,54–56]. Thus, there is consistent evidence that GGBFS reduces both the free chloride and the OH^- concentrations. This effect is not similar in silica fume blends where the Cl^- concentration was observed to steeply increase.

3.4. Effect on corrosion current

The superior corrosion resistance performance in the GGBFS concretes in chloride environments and where calcium hydroxide is very little or totally depleted is of great interest. Rasheeduzzafar et al. [42] have observed the superior corrosion performance of microsilica blends compared to OPC pastes, despite the fact that the Cl^-/OH^- ratio in the silica fume blends has been four to five times its value for plain OPC paste. They attributed this improvement to the densification of the matrix due to the pozzolanic reactions. Nevertheless, the present authors believe that the refinement in the pore structure as shown in Fig. 4 is too small to account for the increased resistance of the blended concrete to chloride initiated corrosion. Results for the corrosion current rate at the depth of 30 mm below the chloride solution, after 2 year ponding, are shown in Fig. 5. The results clearly demonstrate the consistent reduction in corrosion current rate as the GGBFS replacement increases. The 10% inclusion of silica fume in a ternary blend with GGBFS is shown to have resulted in a further reduction in corrosion rate. The reduction recorded for the binary blend that contained 70% GGBFS was 68% compared to the plain OPC concrete. The reduction obtained in the case of the ternary blend with 10% silica fume and 70% GGBFS was 84%. It is important to note here that in contrast to these differences

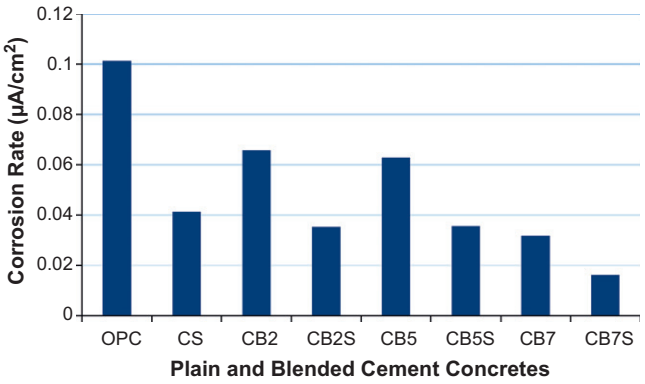

Fig. 5. Corrosion rate in the reinforcement of slabs after 2 year controlled environment exposure.

in corrosion current as affected by the inclusion of GGBFS and/or silica fume, the results of total chloride content at the level of reinforcement were hardly different for the different concretes tested here. The fact that total chloride is nearly the same for all concretes at that particular depth, which is in the range of the cover to the reinforcement, indicates that permeability through these concretes is more or less similar. Yet, it is likely that the free chloride availability in these concretes, as indirectly indicated by the RCPT and the corrosion current values, are different and have been clearly affected by the inclusion of GGBFS and/or silica fume. This observation further emphasises that it is not total chloride that matters, as far as chloride induced corrosion is concerned. It is rather the free chlorides available in the pore solution. If ingressing chloride ions are bound, then that is how protection against this type of corrosion may be achieved.

It is also of considerable interest to observe that the fall in corrosion current has occurred while the environment surrounding the steel has undergone a large reduction in OH^- ions. It could be argued that in the case of GGBFS blends, the reduction in free Cl^- ions may have matched or exceeded the reduction in OH^- and thus the ratio of Cl^-/OH^- may have ended up too low to initiate or maintain an appreciable corrosion current. This result further supports previous findings [9,57] that it is the Cl^-/OH^- ratio that is of paramount importance when it comes to the chloride initiated corrosion. Page et al. examined GGBFS–OPC pastes with admixed chloride solution and found that the free chloride content was drastically reduced as a result of GGBFS presence [9]. They also found that OH^- ion was nearly halved. The Cl^-/OH^- ratios obtained in their testing were 0.112 and 0.061 for OPC and OPC–GGBFS pastes respectively. These results were reflected in the corrosion performance where the OPC–GGBFS paste performed significantly better than plain OPC paste [9]. It also could be inferred from their work that the difference in alumina content had a decisive role in the effect on corrosion resistance. GGBFS composition in the Page et al. series contained 10.8% Al_2O_3 compared to 5.1% in the OPC referred to above in their test. It is well established that alumina has a decisive effect in binding chlorides into Friedel's salt and thus reducing their presence as free ions.

3.5. Role of hydrotalcite

It may be concluded that while silica fume helped to refine the pore structure, the GGBFS effect was to effectively bind the free chlorides. The mechanisms through which the binding of chloride in GGBFS blends occurs, have not been fully explored. One mechanism of chloride binding is known to be the formation of Friedel's salt as a result of a relatively large Al_2O_3 content in the GGBFS, coupled with the availability of calcium and iron oxides. However, it is questionable whether the formation of Friedel's salt and fine pore microstructure are really sufficient for the remarkable improvement in chloride binding in GGBFS concrete. This question becomes of greater importance when it is noticed that this conclusion is supported by the superior performance of high proportion replacement GGBFS concretes compared to fly ash blended concretes of similar proportions [15].

GGBFS contains a significant proportion of magnesia which can be as high as 12% [58]. Magnesia contributes to form hydrotalcite during hydration [16,17] and it can adsorb chloride ions by its distinct anion exchange property [20]. Therefore, the authors believe that hydrotalcite is the hydration product which is responsible for the remarkable improvement in chloride binding by concrete containing GGBFS. In order to verify this hypothesis, the authors conducted a five phase investigation. The preliminary phase has been to measure the chloride adsorbing ability when plain calcined hydrotalcite is subjected to chloride solution. The chloride removal ability of calcined hydrotalcite as a function of time is illustrated in Fig. 6. The chloride ion removal ratio was 40% after 1 h of contact and gradually increased with time. However, the incremental increase in chloride removal ratio was not large. At 24 h reaction time, the chloride removal ratio was about 54%. This duration was then selected as the appropriate time needed for comparing the effect of varying the quantity of hydrotalcite. Fig. 7 displays the chloride removal ratio as a function of added hydrotalcite while keeping the reaction time constant at 24 h. Increasing the quantity of calcined hydrotalcite resulted in increasing the chloride removal ratio. The value of 72% chloride ion removal was recorded when the dose of plain calcined hydrotalcite was 16 g in 80 mL solution. This reflects the high efficiency of hydrotalcite in binding chloride ions in saline solutions. This result strongly supports the argument that if hydrotalcite is produced during the hydration of GGBFS concrete, it would play an important role in binding the otherwise free chloride when the concrete structures are exposed to chloride laden environments.

The second phase has been the identification of hydrotalcite mineral formation in pure GGBFS pastes using X-ray diffraction (XRD). The XRD patterns for a paste activated with 4M NaOH at different ages are shown in Fig. 8a. The highest peak at around 29.5° could be easily identified to indicate the formation of calcium silicate hydrate, and a poorly crystalline calcium silicate hydrate was also observed at around 50°. As expected and reported in the literature, the highest peak observed for hydrotalcite was at 11.5° [59,60]. The second highest peak appeared at 22.9° while the other minor peaks were at 34.7°, 39.1°, 46.4°, 60.6° and 61.9°. Further-

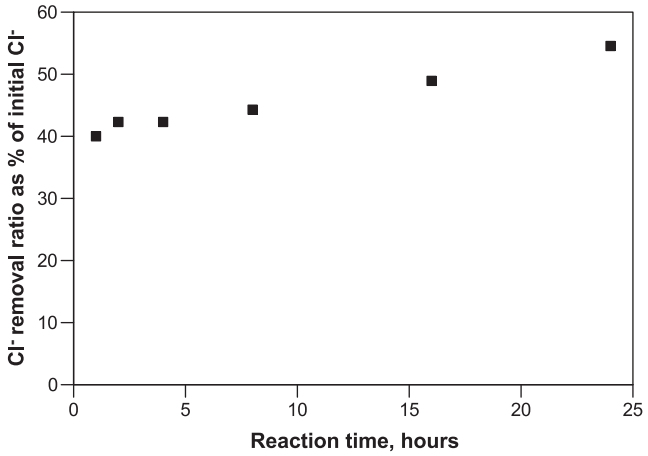

Fig. 6. Removal of chloride ions by calcined hydrotalcite as a function of contact time.

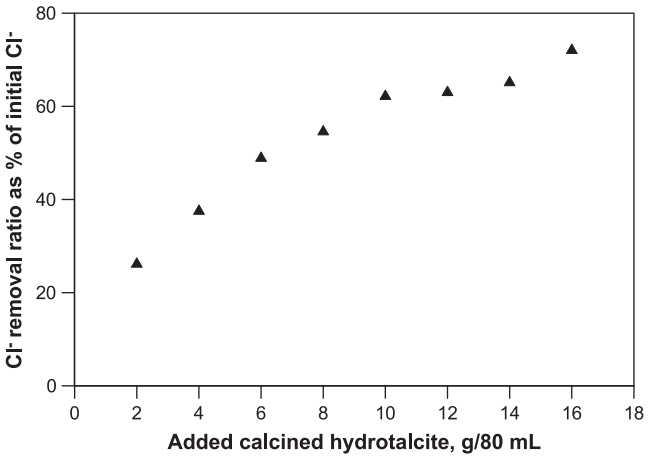

Fig. 7. Chloride ion removal ratio as a function of quantity of calcined hydrotalcite.

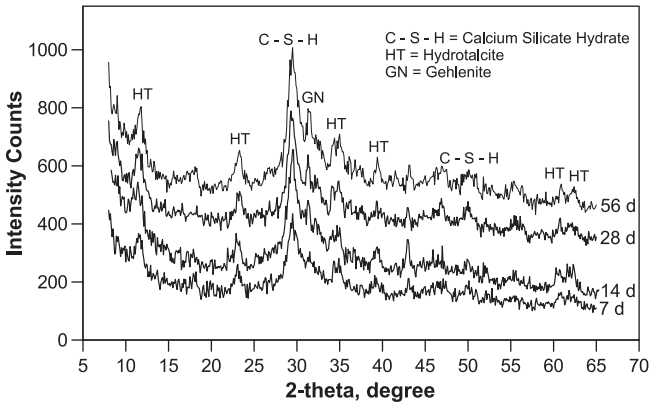

Fig. 8a. XRD patterns of GGBFS pastes activated with 4M NaOH (Note: in order to distinguish the four XRD traces, the traces of the 14, 28 and 56 days pastes were shifted upward by 50, 225 and 350 units, respectively).

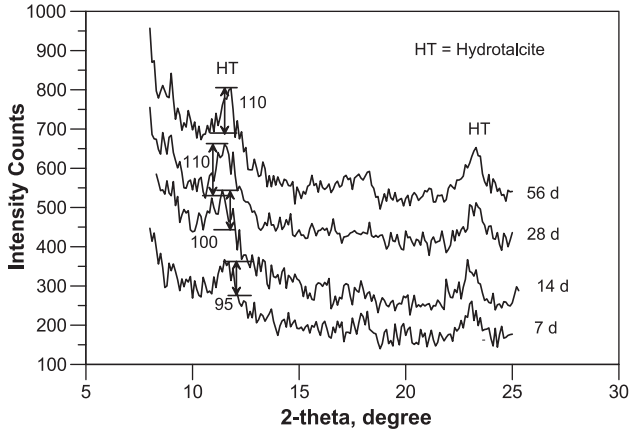

Fig. 8b. Enlarged section of Fig. 8a showing the relative intensity count values.

more, aluminium rich gehlenite was also formed as indicated at 31°. It is noticeable that no calcium hydroxide formation is recorded as a hydration product of GGBFS. This is expected as calcium hydroxide would have been consumed by pozzolanic reactions to produce additional calcium silicate hydrate gel.

In the third phase, chloride was added to pure calcined hydrotalcite in order to investigate whether other crystal formations

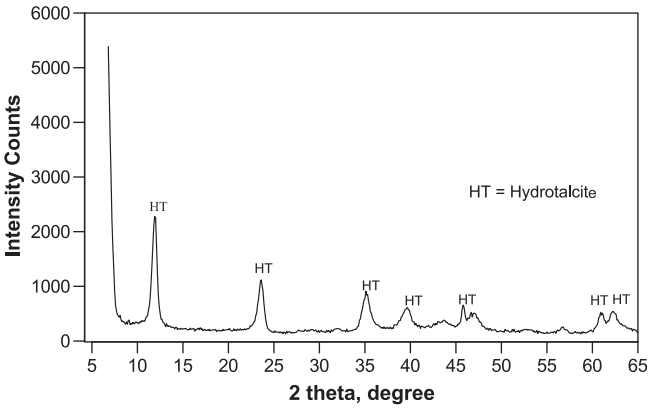

Fig. 9. XRD patterns of calcined hydrotalcite mixed with chlorides.

could be observed during the reaction between calcined hydrotalcite and chlorides. Fig. 9 reveals that the XRD pattern for calcined hydrotalcite with chlorides is identical with the pattern reported by Narayanan and Krishna for calcined hydrotalcite without chlorides [60]. This result confirmed that the structure of hydrotalcite remained unchanged after adsorbing chlorides by replacing interlayer anions.

In the fourth phase, chloride solution was added with GGBFS during mixing to observe whether Friedel's salt formed in addition

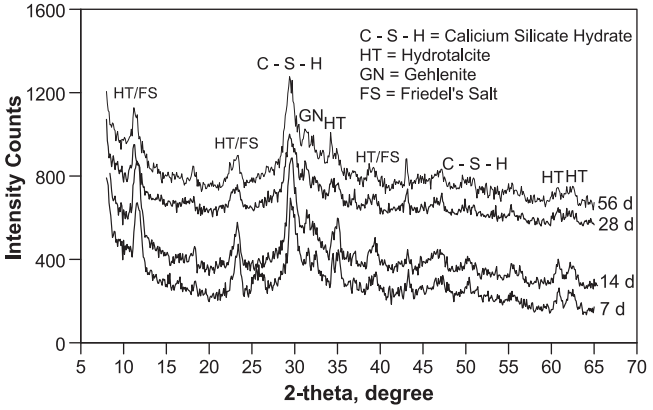

Fig. 10a. XRD patterns of GGBFS pastes mixed with 1.5% Cl^- (Note: in order to distinguish the four XRD traces, the traces of the 14, 28 and 56 days pastes were shifted upward by 100, 430 and 500 units, respectively).

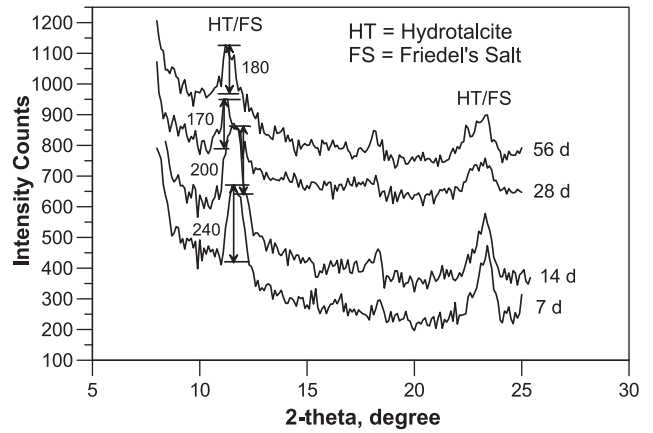

Fig. 10b. Enlarged section of Fig. 10a showing the relative intensity count values.

Table 3
Relative quantities of the crystalline phases formed in hardened plain GGBFS paste and cement-50% GGBFS paste, both activated by 4M NaOH.

Sample type	Hydrotalcite (%)	Tobermorite (%)	Gehlenite (%)	Portlandite (%)	Hatrurite (%)	Quartz (%)
4M_GGBFS	53.94	37.26	8.39	–	–	0.41
4M_GGBFS50	20.17	51.65	–	9.08	19.10	–

to hydrotalcite during the reaction between tri-calcium aluminate phases (C_3A) and chlorides. Fig. 10a presents the XRD patterns of GGBFS pastes activated by 4 M NaOH and with 1.5% chloride content added by mass of GGBFS. The highest peak was observed at 29.5° identifying the formation of calcium silicate hydrate similar to the case of GGBFS pastes activated by 4M NaOH without any chloride. It is however, very difficult to identify Friedel's salt in this case, as the XRD pattern for Friedel's salt coincides with that of hydrotalcite at about 11.5°, 22.9° and 39.1° [61]. However, the peaks in these three positions were higher than the peaks for hydrotalcite in pastes without chloride. This observation is further illustrated in Figs. 8b and 10b where the portion of the graphs between $2\theta = 8°$ and $2\theta = 25°$ is enlarged and thus allowing to show and compare the heights of the relevant peaks. This indicates that formation of Friedel's salt is also likely to occur during hydration of GGBFS in the presence of chloride and calcium oxide. Furthermore, hydrotalcite was also identified in Fig. 10a at 34.7°, 60.6° and 61.9° as it was also shown in Figs. 9 and 8a. For these latter peaks, the peak heights in Figs. 8a and 10a are similar.

In the fifth phase, quantification of hydrotalcite in hydrated GGBFS paste was performed. XRD analysis was conducted at the age of 56 days, on hardened GGBFS which was activated by 4M NaOH. The quantification obtained using the method described earlier in this paper (Section 2.7), is summarised in Table 3. In this Table, it can be seen that hydrotalcite comprised 53.94% of the crystallised phases. Thus, hydrotalcite makes the highest proportion of the crystalline phases in hardened GGBFS paste. Its proportion is followed by the crystalline phase of C–S–H which makes 37.26% of the total crystalline phases. Furthermore, XRD analysis and quantification of the crystalline phases were carried out on 56 day old 50% GGBFS-Portland cement blend, referred to as 4M_GGBFS50. The XRD analysis for this blend is depicted in Fig. 11 which clearly shows that hydrotalcite is formed in binary blend pastes. The quantification presented in Table 3 shows that the 50% GGBFS replacement of Portland cement resulted in hydrotalcite proportion becoming 20.17% compared to the tobermorite crystalline phase being 51.65%. It however, needs to be emphasised that the quantification presented here accounts only for the crystalline phases and their proportions within the total crystalline material excluding the amorphous products.

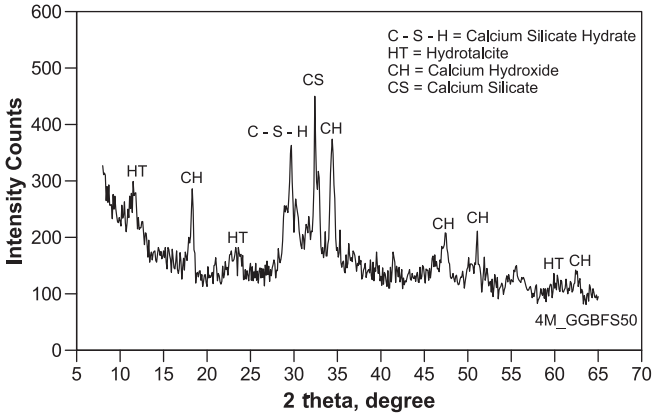

Fig. 11. XRD pattern of 4M_GGBFS50 paste at 56 days.

From the above discussion, it may be seen that hydrotalcite possesses a strong capability to adsorb chloride ions. It has also been shown that hydrotalcite is the largest crystalline formation amongst the crystalline phases of the products of plain GGBFS hydration reactions. Thus, it may be concluded that hydrotalcite must be a significant factor in binding free chloride ions as they penetrate into GGBFS concrete.

4. Conclusions

(1) High volume replacements of Portland cement by ground granulated blast furnace slag resulted in significant reductions in the conductivity of the concrete (measured as electric charge passed) as indicated by the RCPT. Ternary blends that contain 10% silica fume together with GGBFS have resulted in further reductions in the electrical conductivity of concrete. Although the reduction in conductivity has been accompanied by a slight reduction in total chloride content due to diffusion, the reduction in total chloride diffusivity is considered too small to be the cause of the significant improvement in corrosion protection. The reduction of electrical conductivity has been quite well reflected in a significant reduction in the corrosion current in embedded steel reinforcement. As chloride initiated corrosion is dependent on the availability of free chlorides in the pore solution adjacent to steel reinforcement, it may be concluded that the RCPT is more indicative of the free chloride availability as well as the pore solution composition and the Cl^--OH^- relationship.

(2) The silica fume substitution level of 10% by mass of total cementitious materials has been shown to result in consistent reductions in the induced electrical charge, as well as in the measured corrosion current. This however, has occurred despite the equally consistent and rather unexpected observation that this proportion resulted in a reduced strength. It is most likely that this proportion has just exceeded the maximum necessary for strength enhancement. Nonetheless, this did not adversely affect the contribution of silica fume towards reducing corrosion current.

(3) The ability of GGBFS to protect against chloride induced corrosion is attributed to the effective binding of free chloride ions. This binding is likely to be achieved by the action of two mechanisms. The first is the formation of hydrotalcite during hydration. This is largely due to the presence of significant amount of magnesia in GGBFS. The second is the formation of Friedel's salt as a result of the alumina present in the slag. The analysis of hydrotalcite effects revealed that hydrotalcite adsorbs a large amount of chloride ions. Furthermore, the XRD analysis has provided evidence that hydrotalcite is formed in GGBFS pastes and its structure remains unchanged when it adsorbs chloride ions. Moreover, quantification of the hydrotalcite formation has shown that it comprises about 54% of the crystallised phase in hardened pure GGBFS paste and thus it possesses the largest proportion of its crystalline formations compared to the crystalline C–S–H at 37%. It is therefore concluded that hydrotalcite is responsible for superior chloride binding ability of GGBFS concrete. The ion exchange property that is already utilised in other engineering and pharmaceutical

applications is thus shown to offer another important advantage in the ability to bind chloride ions and thus protect against reinforcement corrosion in concrete structures.

(4) Compounds of mixed metal layered hydroxides (MMLH) that are hydrotalcite-like are believed to be a major cause of the binding of chloride, as well as hydroxide ions and thus preventing such ions from being available in the pore solution. It is likely that the binding of the hydrotalcite-like compounds is more efficient in binding chlorides than it is in binding OH^- and thus the net result of a lower Cl^-/OH^- ratio is expected to be obtained in the case of GGBFS blended cements than in the case of straight ordinary Portland cement. It may be further inferred that natural or synthetic hydrotalcite may also be used to protect concrete reinforcement from corrosion. Furthermore, the use of GGBFS, which is essentially an industrial by-product and, as has been shown here to produce hydrotalcite when used in concrete, may add an environmental benefit to its contribution to concrete durability.

(5) The mechanism referred to in the previous paragraph explains the action of ground granulated blast furnace slag and is supported by previously reported evidence of a reduction in the Cl^-/OH^- ratio in the pore solution of OPC-slag blends. However, the action of silica fume in similar conditions needs further research. This is because the presence of silica fume results in a large increase in free chloride ions, associated with a large decrease in free OH^- ions, and thus a very large increase in the Cl^-/OH^- ratio. While it is true that limited silica fume presence decreases porosity and hinders ion mobility, it is considered insufficient to counterbalance the increase of the Cl^-/OH^- ratio. Further research in this area is, therefore needed.

Acknowledgements

The authors wish to thank and acknowledge Ms Ulrike Troitzsch of the Research School of Earth Sciences at the Australian National University for her great help, expertise and advice in the application and analysis of XRD and the relevant software.

References

[1] Kayali O, Haque MN, Khatib JM. Sustain Emer Concr Mater Their Relevance Middle East Open Construct Build Technol J 2008;2:103–10.
[2] Scrivener KL, Bentur A, Pratt PL. Quantitative characterization of the transition zone in high strength concrete. Adv Cem Res 1988;1:230–7.
[3] Hooton RD. Influence of silica fume replacement of cement on physical properties and resistance to sulfate attack, freezing and thawing, and alkali-silica reactivity. ACI Mater J 1993;90:143–51.
[4] Alexander MG, Magee BJ. Durability performance of concrete containing condensed silica fume. Cem Concr Res 1999;29:917–22.
[5] Chindaprasirt P, Rukzon S. Strength, porosity and corrosion resistance of ternary blend Portland cement, rice husk ash and fly ash mortar. Construct Build Mater 2008;22:1601–6.
[6] Ganjian E, Pouya HS. The effect of persian Gulf tidal zone exposure on durability of mixes containing silica fume and blast furnace slag. Construct Build Mater 2009;23:644–52.
[7] Fajardo G, Valdez P, Pacheco J. Corrosion of steel rebar embedded in natural pozzolan based mortars exposed to chlorides. Construct Build Mater 2009;23:768–74.
[8] Shi C. Effect of mixing proportions of concrete on its electrical conductivity and the rapid chloride permeability test (ASTM C1202 or ASSHTO T277) results. Cem Concr Res 2004;34:537–45.
[9] Page CL, Short NR, Holden WR. The influence of different cements on chloride-induced corrosion of reinforcing steel. Cem Concr Res 1986;16:79–86.
[10] Page CL, Vennesland O. Pore solution composition and chloride binding capacity of silica fume-cement pastes. Mater Struct 1983;16:19–25.
[11] Ingerslev LCF. Precast concrete for the Bahrain causeway. Concr Int 1989;11:15–20.
[12] Connell M. The long term performance of high slag concrete. Concr (London) 1998;32:30–1.
[13] Dhir RK, El-Mohr MAK, Dyer TD. Chloride binding in GGBS concrete. Cem Concr Res 1996;26:1767–73.
[14] Luo R, Cai Y, Wang C, Huang X. Study of chloride binding and diffusion in GGBS concrete. Cem Concr Res 2003;33:1–7.
[15] Ahmed MS. Effects of systematic increase of pozzolanic materials on the mechanical, durability, and microstructural characteristics of concrete. Canberra: The University of New South Wales; 2007.
[16] Taylor HFW. Cement chemistry. London: Thomas Telford; 1997. 480 pp.
[17] Hewlett PC. Lea's chemistry of cement and concrete. 4th ed. Elsevier; 2004. 1057pp.
[18] Miyata S. Physico-chemical properties of synthetic hydrotalcite in relation to composition. Clays Clay Miner 1980;28:50–6.
[19] Douglas G, Wendling L, Pleysier R, Trefry M. Hydrotalcite formation for contaminant removal from ranger mine process water. Mine Water Environ 2010;29:108–15.
[20] Patel SH. Processing Aids. In: Xanthos M, editor. Functional fillers for plastics. Wiley; 2005. p. 367–80 [chapter 20].
[21] Hydrotalcite BejoyN. The clay that cures. Resonance 2001;6:57–61.
[22] Lin JK, Uan JY. Formation of Mg, Al-hydrotalcite conversion coating on Mg alloy in aqueous HCO_3^-/CO_3^{2-} and corresponding protection against corrosion by the coating. Corros Sci 2009;51:1181–8.
[23] Wang J, Li D, Yu X, Jing X, Zhang M, Jiang Z. Hydrotalcite conversion coating on Mg alloy and its corrosion resistance. J Alloys Compd 2010;494:271–4.
[24] Álvarez D, Collazo A, Hernández M, Nóvoa XR, Pérez C. Corrosion protective properties of hydrotalcites doped hybrid sol–gel coatings on aluminium substrates. Mater Sci Forum 2010;636–637:996–1003.
[25] Buchheit RG, Guan H, Mahajanam S, Wong F. Active corrosion protection and corrosion sensing in chromate-free organic coatings. Prog Org Coat 2003;47:174–82.
[26] Lv L, He J, Wei M, Evans DG, Duan X. Uptake of chloride ion from aqueous solution by calcined layered double hydroxides: equilibrium and kinetic studies. Water Res 2006;40:735–43.
[27] AASHTO. Standard method of sampling and testing for total chloride ion in concrete and concrete raw materials. American Association of State Highway and Transporation Officials Standards; T-260; 1984.
[28] AASHTO. Standard method of test for electrical indication of concrete's ability to resist chloride ion penetration, T-277; 2007.
[29] ASTM. Electrical indication of concrete's ability to resist chloride-ion penetration; 1991.
[30] Hale M, Russell BM, Bush TD. An assessment of the rapid chloride ion penetrability test. Thomas Telford; 2002.
[31] Ahmed MS, Kayali O, Anderson W. Chloride penetration in binary and ternary blended cement concretes as measured by two different rapid methods. Cem Concr Compos 2008;30:576–82.
[32] AASHTO. Standard method of test for resistance of concrete to chloride ion penetration. T259; 1990.
[33] Pfiefer DW, McDonald DB, Krauss PD. The rapid chloride permeability test and its correlation to the 90 day chloride ponding test. PCI J 1994;39:38–47.
[34] Ahmed MS, Kayali O. Evaluating fly ash blended cements using rapid chloride permeability and long-term testing methods. Concrete Institute of Australia; 2007.
[35] Wajima T, Shimizu T, Ikegami Y. New simple process of making agricultural cultivation solution from seawater. Bullet Soc Sea Water Sci, Jpn 2006;60:201–2.
[36] Hunter BA. Rietica – a visual Rietveld program. Comm Powder Diffract Newslett 1998;20:21.
[37] Rietveld HM. A profile refinement method for nuclear and magnetic structures. J Appl Crystallogr 1969;2:65–71.
[38] Peterson VK, Ray A, Hunter BA. Influence of minor phase inclusion in the Rietveld analysis of cement clinker. Cement and Concrete Institute of South Africa; 2003.
[39] Scrivener KL, Fullmann T, Gallucci E, Walenta G, Bermejo E. Quantitative study of Portland cement hydration by X-ray diffraction/Rietveld analysis and independent methods. Cem Concr Res 2004;34:1541–7.
[40] Broomfield JP. Corrosion rate measurements in reinforced concrete structures by a linear polarization device, vol. 151. ACI Special Publication; 1994. p. 163–182.
[41] Andrade C, Alonso C. On-site measurements of corrosion rate of reinforcements. Construct Build Mater 2001;15:141–5.
[42] Rasheeduzzafar, Ehtesham Hussain S, Al-Gahtani AS. Pore solution composition and reinforcement corrosion characteristics of microsilica blended cement concrete. Cem Concr Res 1991;21:1035–48.
[43] Vedalakshmi R, Rajagopal K, Palaniswamy N. Longterm corrosion performance of rebar embedded in blended cement concrete under macro cell corrosion condition. Construct Build Mater 2008;22:186–99.
[44] Kawamura M, Takemoto K. Correlation between pore solution composition and alkali silica expansion in mortars containing various fly ashes and blasfurnace slags. Int J Cem Compos Lightweight Concr 1988;10:215–23.
[45] Gu P, Beaudoin JJ, Zhang MH, Malhotra VM. Performance of reinforcing steel in concrete containing silica fume and blast-furnace slag ponded with sodium chloride solution. ACI Mater J 2000;97:254–62.
[46] Baweja D, Roper H, Sirivivatnanon V. Chloride-induced steel corrosion in concrete: Part 1 – Corrosion rates, corrosion activity, and attack areas. ACI Mater J 1998;95:207–17.
[47] Larbi JA, Fraay ALA, Bijen J. The chemistry of the pore fluid of silica fume-blended cement systems. Cem Concr Res 1990;20:506–16.

[48] Canham I, Page CL, Nixon PJ. Aspects of the pore solution chemistry of blended cements related to the control of alkali silica reaction. Cem Concr Res 1987;17:839–44.
[49] Rasheeduzzafar, Ehtesham Hussain S. Effect of microsilica and blast furnace slag on pore solution composition and alkali-silica reaction. Cem Concr Compos 1991;13:219–25.
[51] Verbeck GJ. Mechanisms of corrosion of steel in concrete, vol. 49. American Concrete Institute Publication SP; 1975. p. 21–38.
[51] Rasheeduzzafar, Al-Saadoun SS, Al-Gahtani AS, Dakhil FH. Effect of tricalcium aluminate content of cement on corrosion of reinforcing steel in concrete. Cem Concr Res 1990;20:723–38.
[52] Glass GK, Reddy B, Buenfeld NR. The participation of bound chloride in passive film breakdown on steel in concrete. Corros Sci 2000;42:2013–21.
[53] Yuan Q, Shi C, Schutter GD, Audenaert K, Deng D. Chloride binding of cement-based materials subjected to external chloride environment- A review. Construct Build Mater 2009;23:1–13.
[54] Arya C, Buenfeld NR, Newman JB. Factors influencing chloride-binding in concrete. Cem Concr Res 1990;20:291–300.
[55] Dhir RK, El-Mohr MAK, Dyer TD. Developing chloride resisting concrete using PFA. Cem Concr Res 1997;27:1633–9.
[56] Arya C, Xu Y. Effect of cement type on chloride binding and corrosion of steel in concrete. Cem Concr Res 1995;25:893–902.
[57] Kayyali OA, Haque MN. The Cl^-/OH^- ratio in chloride-contaminated concrete – a most important criterion. Mag Concr Res 1995;47:235–42.
[58] Lumley JS, Gollop RS, Moir GK, Taylor HFW. Degrees of reaction of the slag in some blends with Portland cements. Cem Concr Res 1996;26:139–51.
[59] Van der ven L, Van Gemert MLM, Batenburg LF, Keern JJ, Gielgens LH, Koster TPM, et al. On the action of hydrotalcite-like clay materials as stabilizers in polyvinylchloride. Appl Clay Sci 2000;17:25–34.
[60] Narayanan S, Krishna K. Structure activity relationship in pd/hydrotalcite: Effect of calcination of hydrotalcite on palladium dispersion and phenol hydrogenation. Catal Today 1999;49:57–63.
[61] Bothe JVJ, Brown PW. PhreeqC modeling of Friedel's salt equilibria at 23 ± 1 °C. Cem Concr Res 2004;34:1057–63.